ISIJ International, Vol. 46 (2006), No. 6, pp. 903–908

Numerical Simulation of Solidification Structure Formation during Continuous Casting in Fe–0.7mass%C Alloy Using Cellular Automaton Method

Minoru YAMAZAKI,[1] Yukinobu NATSUME,[1] Hiroshi HARADA[2] and Kenichi OHSASA[1]

1) Graduate School of Engineering, Hokkaido University, N13,W8, Kita-ku, Sapporo 060-8628 Japan.
2) Nippon Steel Corporation, Fujicho-1, Hirohata-ku, Himeji 671-1188 Japan.

(*Received on January 10, 2006; accepted on April 4, 2006*)

A numerical model was developed for the simulation of solidification structure formation during the continuous casting process of an Fe–0.7mass%C alloy. In this model, the cellular automaton method was combined with heat transfer calculation during the continuous casting process. The effect of electromagnetic stirring (EMS) during the continuous casting process was introduced as an increase in thermal conductivity in liquid. Furthermore, the effect of fragmentation of dendrites due to fluid flow during EMS was taken into account in the model as an increase in the formation of crystals. Simulations of grain structure formation in continuously cast billets with and without EMS were carried out, and the degree of fragmentation was evaluated from a comparison between experimentally observed and simulated macrostructures of the billets.

KEY WORDS: numerical simulation; cellular automaton method; solidification structure; carbon steel; continuous casting; electromagnetic stirring; fragmentation.

1. Introduction

Control of the solidification structures of a casting and ingot is important because the solidification structure has influences the mechanical properties of final products. To predict the optimum conditions to obtain a desired solidification structure, it is important to clarify the effects of the process parameters on the solidification structure. However, many experimental works would be required to obtain optimum conditions. Hence, it is desirable to develop a mathematical model to simulate solidification structure formation in a casting and ingot. In the past two decades, several models for prediction of solidification structure formation have been developed. Stochastic models such as the Monte Carlo (MC) method[1] and cellular automaton (CA) method[2,3] and deterministic models such as the phase-field (PF) method[4–8] have been presented, and many attempts have been carried out to simulate solidification structure formation of alloys using these methods.

However, there have been few attempts to simulate solidification structure formation in steel, which is the most widely used material in the world. For this reason, two factors might be considered. First, steels are mostly produced by the continuous casting process and solidification must proceed under flow in melt due to electromagnetic stirring (EMS) in the usual continuous casting process. This condition makes modeling of solidification structure formation in steel difficult. Second, during the solidification of steel, complex phase transformations such as peritectic reaction and subsequent peritectic transformation occur. These phenomena also make modeling of solidification structure formation in steel difficult.

The aim of this work was to develop a numerical model to simulate solidification structure formation in an Fe–C binary alloy during a continuous casting process. In the model, the effect of fluid flow due to EMS was taken into account. To avoid the difficulty in treating the peritectic reaction and peritectic transformation, an Fe–0.7mass%C binary alloy without peritectic reaction was chosen as the target alloy in this model. The effect of fluid flow on solidification structure of the Fe–0.7mass%C alloy during the continuous casting process was examined by using the developed model.

2. Numerical Model

In the present model, the cellular automaton method (CA) was combined with heat transfer calculation during the continuous casting process. The procedure for simulation by the CA method is basically the same as that by the CA technique developed by Rappaz and Gandin[2] except for the nucleation model. The CA procedure in the present model was carried out under the temperature field obtained by heat transfer calculation.

2.1. Nucleation Model

The Gaussian distribution reported by Thevoz *et al.*[9] has been widely used as a nucleation model in the CA method. In this nucleation model, if the mold wall and bulk liquid are considered as nucleation sites, six parameters must be

determined. This makes the model complicated and interpretation of the physical meaning of each parameter is difficult.

In the present work, a simple nucleation model was used, and the heterogeneous nucleation rate in undercooled melt, R_{Nu}, is expressed as follows:

$$R_{Nu}(\Delta T)=\frac{1}{\Delta t\cdot V_{CA}}\left(\frac{\Delta T}{a}\right)^{n} \quad \text{.....(1)}$$

where Δt is the time step, V_{CA} is the area of a CA cell, ΔT is undercooling, a is maximum undercooling for nucleation and exponent, n, is the nucleation parameter. It has been demonstrated that the use of a combination of a fixed value of a and a variable n is effective for simulation of solidification structure formation.[10] In this nucleation model, the fitting parameter is only the exponent, n for a constant value of a.

Equation (1) expresses the rate of heterogeneous nucleation in the bulk liquid. On the other hand, at the mold wall, it is assumed that nucleation always occurs in the liquid CA cell in contact with the mold wall if the cell is in an undercooled state. This assumption is reasonable because it is expected that the potential of heterogeneous nucleation at the mold wall is considerably higher than that in the bulk liquid.

2.2. Growth Kinetics

The KGT (Kurz, Givoanola, Trivedi) model[11,12] was used as the model of growth kinetics of a dendrite tip in an Fe–C binary alloy. Based on the marginal stability criterion, one obtains

$$V^2A+VB+C=0 \quad \text{.....(2)}$$

with

$$A=\frac{\pi^2\Gamma}{P_C^2D^2}$$

$$B=\frac{mC_0(1-k_0)\xi_C}{D[1-(1-k_0)Iv(P_C)]}$$

$$C=G$$

where V is the growth velocity of a dendrite tip, Γ is the Gibbs-Thomson coefficient, P_C is the Peclet number for solute diffusion, D is the diffusion coefficient in liquid, m is the liquidus slope, C_0 is the initial concentration, k_0 is the partition coefficient, $Iv(P_C)$ is the Ivantsov function and G is the temperature gradient. $\xi_C=\pi^2/(k_0P_C)$ and it close to unity at low growth velocity. For the dendrite growth regime, the imposed temperature gradient, G, has little effect on the growth velocity and can be regarded as zero.

Temperature at the dendrite tip, T_{tip}, was expressed as follows:

$$T_{tip}=T_0+mC_0\left[\frac{1}{1-(1-k_0)Iv(P_C)}\right]-\frac{2\Gamma}{r} \quad \text{.....(3)}$$

where T_0 is the melting point of pure Fe and r is the dendrite tip radius. The relationship between the undercooling, ΔT, at the dendrite tip and the growth velocity can be calculated from the Eqs. (2) and (3) by substituting an arbitral value of the Peclet number for Eqs. (2) and (3).

To reduce the simulation time, the set of values for undercooling *vs*. growth velocity of the dendrite tip were calculated from Eqs. (2) and (3) in advance and then formulated as the form of Eq. (4) by using the least-square method.

$$V(\Delta T)=2.0\times10^{-4}\cdot\Delta T^4+4.6\times10^{-3}\cdot\Delta T^3+3.54\times10^{-3}\cdot\Delta T^2+7.56\times10^{-2}\cdot\Delta T \quad \text{.....(4)}$$

where $V(\Delta T)$ is the growth velocity of the dendrite tip (mm/s) and ΔT is undercooling. The material properties used in the calculation are listed in **Table 1**.

Table 1. Materials properties of the Fe–C binary alloy used in the simulation.

Symbol	Value
T_0	1801 K
m	-65
k_0	0.353
Γ	1.9×10^{-7}(Km)
D	2.0×10^{-8}(m^2/s)

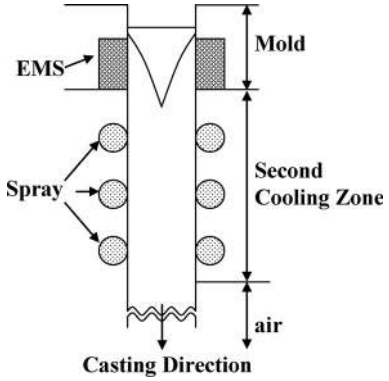

Fig. 1. Schematic illustration of boundary conditions used for the heat transfer calculation of the continuous casting process of an Fe–C binary alloy billet.

2.3. Heat Transfer Calculation during Continuous Casting

Equation (5) shows the governing equation for 2-dimensional heat transfer calculation.

$$\frac{\partial T}{\partial t}=\frac{\kappa}{\rho C_p}\left(\frac{\partial^2T}{\partial x^2}+\frac{\partial^2T}{\partial y^2}\right) \quad \text{.....(5)}$$

where κ is thermal conductivity, ρ is density and C_p is specific heat. The evolution of latent heat during the solidification was incorporated to the calculation by using the effective specific heat method as shown in the following equation.

$$C_p'=C_p-L\left(\frac{df_S}{dT}\right) \quad \text{.....(6)}$$

where C_p' is the effective specific heat, L is latent heat and f_s is the solid fraction.

Figure 1 shows the boundary conditions of the heat

Table 2. Thermopysical properties and heat transfer coefficients used in the simulation. h_{mold} is the heat transfer coefficient at the mold wall, and h_{S1} (0–0.1 m), h_{S2} (0.1–0.9 m), h_{S3} (0.9–2.2 m) and h_{S4} (2.1–4.4 m) are the heat transfer coefficients at the secondary cooling zone. Figures in parentheses are distances from the bottom of the mold. z is the distance from the top of the mold, and v is casting speed.

Symbol	Value
κ	28.5W/m K
ρ	7000kg/m^3
C_P	0. 645J/kg K
L	0.268J/kg
h_{Mold}	$1256 \times \exp(1.31 \times z/(v \times 60))$ W/m^2 K
h_{S1}(0-0.1m)	1248W/m^2 K
h_{S2}(0.1-0.9m)	758W/m^2 K
h_{S3}(0.9-2.1m)	582W/m^2 K
H_{S4}(2.1-4.4m)	427W/m^2 K

transfer calculation during the continuous casting process. A billet was moving down from the mold, and the sample was first cooled in the mold by heat transfer from the sample to the mold. The sample was then cooled at the secondary cooling zone by spray, and this zone was divided into four zones with different heat transfer conditions to enhance the accuracy of the heat transfer calculation. Finally, the sample was cooled in air, and the heat extraction from the sample in this regime was calculated by radiation. In the heat transfer calculation, the heat flow condition at the surface of the billet was changed with lapse of time by synchronizing with the movement of the billet. The thermophysical properties and the heat transfer coefficients in the mold and the secondary cooling zones used in the calculation are shown in **Table 2**.

2.4. Effect of EMS

Electromagnetic stirring (EMS) is generally used to reduce the centerline segregation in the continuous casting process. To evaluate the effect of the fluid flow due to EMS on heat flow in the billet, the accurate flow pattern in the molten steel melt must be known. However, at present, it is difficult to combine accurate calculation of fluid flow with heat transfer calculation and the CA procedure due to very large computational load.

A method has been reported for incorporating the effect of fluid flow into heat transfer calculation by changing thermal conductivity.[13,14] In this method, apparent thermal conductivity in molten steel with EMS becomes larger than that without EMS. In the present study, this method was used to calculate the heat transfer in the billet with EMS. In the calculation, regions in which fluid flow can occur were determined according to the classification of solid–liquid coexisting zone proposed by Takahashi *et al.*[15]

Figure 2 shows a schematic illustration of solid–liquid coexisting zone of a solidifying alloy. The solid–liquid coexisting zone was classified into three zones of q_2, q_1 and p based on the fluidity of interdendritic liquid. In the q_2 zone, primary crystals and liquid can flow concurrently, whereas only interdendritic liquid can flow among dendrites in the q_1 zone and the liquid is entrapped by solids and can not flow in the p zone.

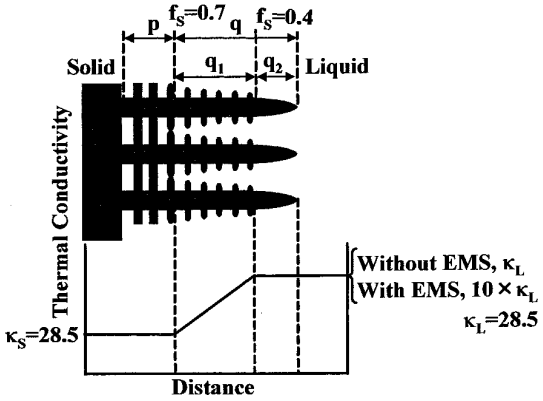

Fig. 2. Schematic illustration of solid–liquid coexisting zones during the solidification of an alloy.

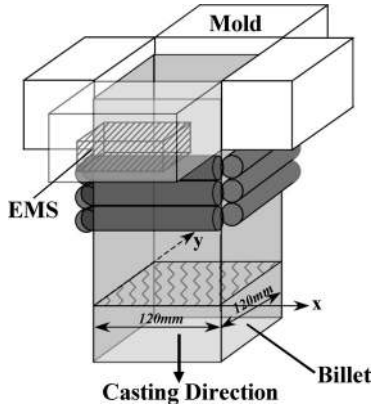

Fig. 3. Schematic illustration of the continuous caster used in the experiment.

In the present work, based on this concept of solid–liquid coexisting zone, the thermal conductivity in solid was used in the region of solid and the p zone, and the effective thermal conductivity in liquid with fluid flow was used in the region of liquid and the q_2 zone. In the q_1 zone, the thermal conductivity changes linearly from liquid to the p zone according to the fraction of liquid that can flow among dendrites as shown in Fig. 2.

Mizikar used a 7.5-times higher thermal conductivity in liquid with fluid flow due to EMS.[13] Although the exact value of the thermal conductivity in liquid with EMS is not clear because the value changes depending on flow velocity in the liquid, a 10-times higher thermal conductivity was assumed as the effective thermal conductivity in liquid with EMS in comparison with the thermal conductivity in liquid without EMS.

3. Calculation Procedure

3.1. Experiment and Simulation Model

To examine the effectiveness of the present model, simulation was carried out under the same conditions as those used in a continuous casting experiment.[16] **Figure 3** shows a schematic illustration of the continuous caster used in the experiment,[16] and experimental conditions are shown in **Table 3**. A vertical type test continuous caster with a machine height of 8 m was used to produce a billet with a size of 120 mm×120 mm, and EMS was applied in a mold. **Figure 4** shows solidification structures in the cross sec-

Table 3. Casting conditions.

Casting Speed	1.5m/min
Steel Grade	0.7mass%C
Superheat	30K

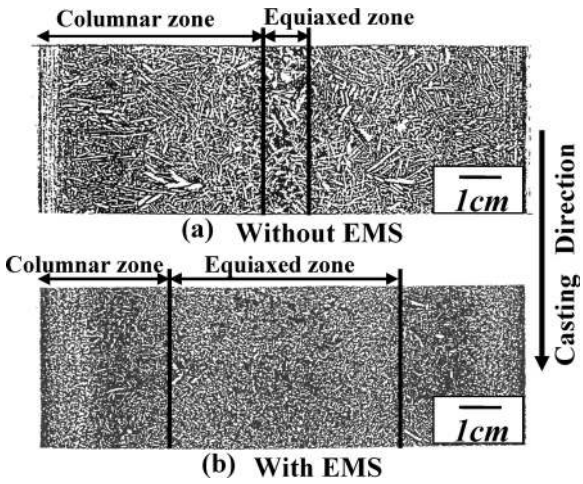

Fig. 4. Experimentally observed solidification structure of a continuously cast billet[16] without EMS (a) and with EMS (b).

tions along with casting direction of continuously cast billets with and without EMS.[16] In the case without the EMS (Fig. 4(a)), columnar grains were formed from the mold surface to the center of the ingot. On the other hand, in the case with EMS (Fig. 4(b)), the region of equiaxed grains was extended due to the effect of EMS.

3.2. Calculation Conditions

To solve Eq. (5) by using the finite difference method, the cross section perpendicular to the casting direction of the billet was divided into rectangular grids with 1.2 mm on x- and y-coordinates. Since the shape of the sample is axial-symmetric, a quarter of the cross section was divided as shown in **Fig. 5**, and calculated thermal field in the quarter was transferred to the other three quarters.

An explicit finite difference method was used, and the time step was determined to be 0.0025 s by considering the stability of the numerical computation. A network of square CA cells was laid on the cross section of the billet, and the heat transfer grids were superimposed on the CA cells as shown in Fig. 5. One heat transfer grid contains 16 CA cells, and the size of a CA cell was 0.3×0.3 mm.

It should be noted that the simulated area of the billet was a cross section perpendicular to the casting direction, whereas the observed macrostructure of the billet in Fig. 4 was a section parallel to the casting direction. However, it is no difficulty for comparison of the simulated and observed microstructures of the billet.

4. Results and Discussion

4.1. Simulation without EMS

Figure 6 shows the simulated macrostructure of the continuously cast billet without EMS. Fine equiaxed grains, *i.e.*, chill crystals, were formed near the mold surface, and columnar grains grew up to the center of the billet. The

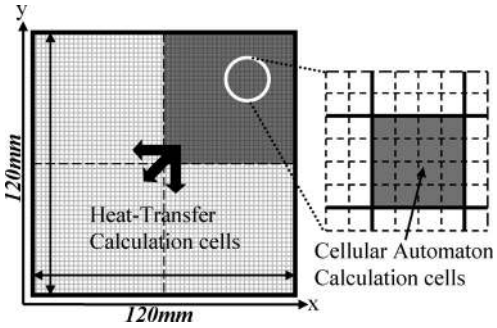

Fig. 5. Numerical grids for heat transfer calculation and CA cells used in the simulation.

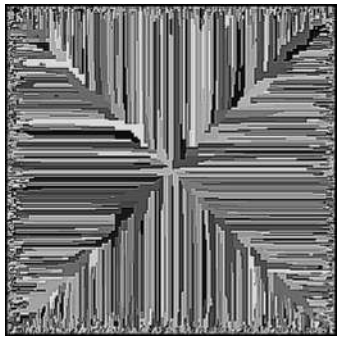

Fig. 6. Simulated solidification structure of the continuously cast billet in an Fe–0.7mass%C alloy without EMS.

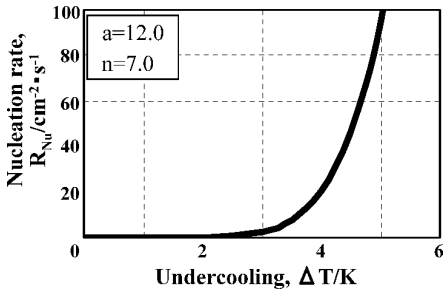

Fig. 7. Relationship between degree of undercooling, ΔT, and nucleation rate, R_{Nu}, used in the simulation without EMS.

structure shown in Fig. 6 was composed mostly of columnar grains, whereas a region of equiaxed grains was observed in the center of the billet obtained by the experiment as shown in Fig. 4(a). **Figure 7** shows the relationship between undercooling and nucleation rate in liquid used in the simulation. A combination of nucleation parameters of $a=12.0$ and $n=7.0$ was used for the nucleation rate, and the resulting relationship between undercooling, ΔT, and nucleation rate, R_{Nu}, is shown in Fig. 7. The value of 'a' was arbitrarily determined, and the value of 'n' was determined as the maximum nucleation rate producing a chill crystal zone similar to that in the experiment. If the nucleation rate was increased more than that shown in Fig. 7, the chill crystal zone was extended, and resulting macrostructure was not similar to the experimentally observed structure. The simulated macrostructure of fully developed columnar crystals can be explained due to relatively low thermal conductivity of steel. A temperature gradient formed in the liquid in front of the solidification front during the solidification of steel becomes steep due to its low thermal conductivity, and

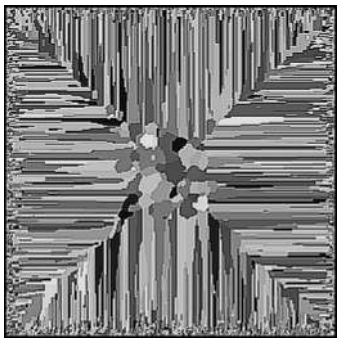

Fig. 8. Simulated solidification structure of the continuously cast billet in an Fe–0.7mass%C alloy with EMS.

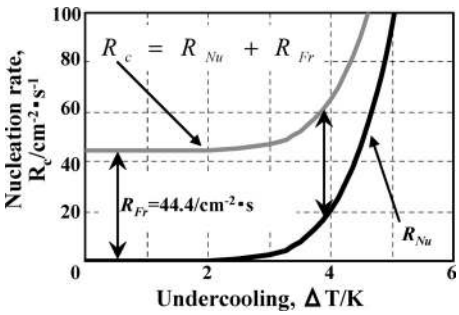

Fig. 9. Relationship between degree of undercooling,ΔT, and total crystal formation rate, R_C, used in the simulation with consideration of the fragmentation of dendrites.

Fig. 10. Simulated solidification structure of a continuously cast billet with consideration of the fragmentation of dendrites.

this means that constitutional undercooling in front of columnar grains hardly occurs. As a result, the formation of equiaxed crystals in front of columnar grains is difficult and columnar grains can grow up to the center of the billet.

The disagreement between simulated and experimentally observed solidification structures might be ascribed to the presence of fluid flow in the solidifying billet due to pouring of molten steel and convection in the experiment. The presence of concentrated heterogeneous nucleation catalysts in the center region of the billet at the final solidification stage might be the reason of the formation of an equiaxed crystal region observed in the experiment.

4.2. Simulation with EMS

Figure 8 shows the simulated macrostructure of the continuously cast billet with EMS. The same nucleation parameters as those used in the simulation without EMS were used in the simulation. In the simulation with EMS, higher thermal conductivity in liquid due to fluid flow was used to introduce the effect of EMS, and a region of equiaxed grains was formed in the center of the billet as shown in Fig. 8. Increased thermal conductivity in liquid ahead of the columnar crystals reduced the temperature gradient in liquid, which enhanced the constitutional undercooling in liquid and resulted in the formation of equiaxed crystals in front of columnar crystals. However, the simulated region of equiaxed crystals at the center of the billet was smaller than that in the experimentally observed solidification structure shown in Fig. 4(b). These results suggested that the effect of EMS is not only change in thermal conductivity in liquid but also promotion of fragmentation of dendrites due to fluid flow.

To take into account the accurate effect of the fragmentation of dendrites, it is necessary to understand the mechanism of fragmentation due to fluid flow. However, at present, it is difficult to make such model.

In the present work, the contribution of fragmentation of dendrites to the multiplication of equiaxed crystals was incorporated into the nucleation model. Total crystal formation rate, R_c, was defined as the sum of the contribution of heterogeneous nucleation in liquid and the contribution due to the fragmentation of dendrites, R_{Fr}.

$$R_c = R_{Nu} + R_{Fr} \quad \text{.....(7)}$$

The value of R_{Fr} was assumed to be independent of the undercooing in melt because the fragmented crystals were moved by the fluid flow, and the number of fragmented crystals could not be related to the undercooling at the position to which the crystals were carried. **Figure 9** shows the relationship between the undercooling, ΔT, in melt and the total crystal formation rate R_c, used in the simulation with EMS. In Fig. 9, heterogeneous nucleation rate, R_{Nu}, was moved upward just by R_{Fr} to express the total crystal formation rate, R_c. In this simulation, the value of parameter R_{Fr} was determined by reproducing the area of equiaxed crystals same as that experimentally observed shown in Fig. 4(b), and the estimated value of R_{Fr} required for the contribution of fragmentation was about 44.4 $cm^{-2}\,s^{-1}$.

Figure 10 shows the simulated macrostructure of a continuously cast billet taking into account the effect of the fragmentation of dendrites due to EMS. A large region of equiaxed grains that was the same as that observed in the experiment was simulated. This result demonstrates the potential of the present model to simulate solidification structure formation during the continuous casting process of steel.

5. Conclusions

A numerical model to simulate solidification structure formation during the continuous casting process of an Fe–C binary alloy was developed by combining heat transfer calculation and the cellular automaton (CA) method. To avoid the difficulty in modeling peritectic transformation, an Fe–0.7mass%C binary alloy without peritectic reaction was chosen as the target alloy. The effect of the fluid flow due to electromagnetic stirring (EMS) was introduced into the model by considering enhanced thermal conductivity in liquid and crystal multiplication due to the fragmentation of

dendrites. Simulations of solidification structure formation during continuous casting with and without EMS were carried out, and the results of simulation were compared with experimental results. In the simulation without EMS, columnar grains grew from the chill zone to the center of the billet, whereas a small region of equiaxed crystals was observed in the experiment. In the simulation with EMS, a solidification structure similar to that observed in the experiment could be simulated by considering both the effects of enhanced thermal conductivity in liquid and the contribution of fragmentation of dendrites due to fluid flow.

REFERENCES

1) J. A. Spittle and S. G. R. Brown: *Acta Metall. Mater.*, **37** (1989), 1803.
2) M. Rappaz and Ch.-A. Gandin: *Acta Metall. Mater.*, **41** (1993), 345.
3) L. Nastac: *Acta Mater.*, **47** (1999), 4253.
4) R. Kobayashi: *Physica D*, **63** (1993), 410.
5) S. G. Kim, W. T. Kim and T. Suzuki: *Phys. Rev. E*, **60** (1999), 7186.
6) Y. Natsume, K. Ohsasa and T. Narita: *Mater. Trans.*, **43** (2002), 2228.
7) Y. Natsume, K. Ohsasa and T. Narita: *Mater. Trans.*, **44** (2003), 819.
8) Y. Natsume, K. Ohsasa, H. Esaka and T. Narita: *Mater. Trans.*, **44** (2003), 824.
9) Ph. Thevoz, J. L. Desbiolles and M. Rappaz: *Metall. Trans.*, **20A** (1989), 311.
10) Y. Natsume and K. Ohsasa: *ISIJ Int.*, **46** (2006), 896.
11) W. Kurz, B. Giovanola and R. Trivedi: *Acta Metall.*, **34** (1986), 823.
12) W. Kurz and D. J. Fisher: Fundamentals of Solidification, fourth revised edition, Trans Tech Publishers, Aedermannsdorf, Switzerland, (1998), 77.
13) E. A. Mizikar: *Trans. Metall. Soc. AIME*, **239** (1967), 1747.
14) T. Takahashi, K. Ohsasa and N. Katayama: *Tetsu-To-Hagané*, **76** (1990), 728.
15) T. Takahashi and I. Hagiwara: *J. Jpn. Inst. Met.* **29** (1965), 1152.
16) H. Harada, K. Miyazawa, T. Matsumiya, T. Morohoshi and H. Esaka: *Tetsu-To-Hagané*, **89** (2003), 265.